
Visual Structures Helps Visual Reasoning: Addressing the Binding Problem in VLMs

Amirmohammad Izadi, Mohammad Ali Banayeeanzade, Fatemeh Askari,
Ali Rahimiakbar, Mohammad Mahdi Vahedi, Hosein Hasani,
and Mahdieh Soleymani Baghshah

Sharif University of Technology

Abstract

Despite progress in Vision-Language Models (VLMs), their capacity for visual reasoning is often limited by the *binding problem*: the failure to reliably associate perceptual features with their correct visual referents. This limitation underlies persistent errors in tasks such as counting, visual search, scene description, and spatial relationship understanding. A key factor is that current VLMs process visual features largely in parallel, lacking mechanisms for spatially grounded, serial attention. This paper introduces a simple yet effective intervention: augmenting visual inputs with low-level spatial structures (e.g., horizontal lines) and pairing this with a textual prompt that encourages sequential, spatially-aware parsing. We empirically demonstrate substantial performance improvements across core visual reasoning tasks. Specifically, our method improves GPT-4o visual search accuracy by 25.00%, increases counting accuracy by 26.83%, reduces edit distance error in scene description by 0.32, and enhances performance on spatial relationship tasks by 9.50% on a 2D synthetic dataset. Furthermore, we find that the visual modification is essential for these gains; purely textual strategies, including Chain-of-Thought prompting, are insufficient and can even degrade performance. Our method enhances binding only with a single-query inference, underscoring the importance of visual input design over purely linguistically-based approaches. These findings suggest that low-level visual structuring is a powerful and underexplored direction for improving compositional visual reasoning and could serve as a general strategy for enhancing VLM performance on spatially grounded tasks.

1 Introduction

Large Language Models (LLMs) have achieved remarkable progress, matching or even surpassing human performance across a range of complex tasks [1–5]. Despite significant advancements, Vision-Language Models (VLMs) still lag behind LLMs in core reasoning capabilities. While LLMs excel at symbolic and abstract reasoning, VLMs struggle with essential aspects of visual understanding. They frequently miscount objects in cluttered or overlapping scenes [6, 7], perform poorly in spatial reasoning (e.g., identifying “left of” or “above”) [8], and often fail to accurately locate or recognize salient targets during visual search [9]. Moreover, compositional and relational reasoning, where understanding critically depends on structured relationships between objects, remains a major challenge [6]. These limitations indicate that VLMs, despite their power, lack key mechanisms for structured visual reasoning. Consequently, their performance in these areas does not yet match that of language-only models in comparable text-based reasoning tasks.

The limitations in visual reasoning tasks can largely be attributed to a fundamental challenge known as the *binding problem* [9]. Originating from cognitive science and neuroscience, the binding problem

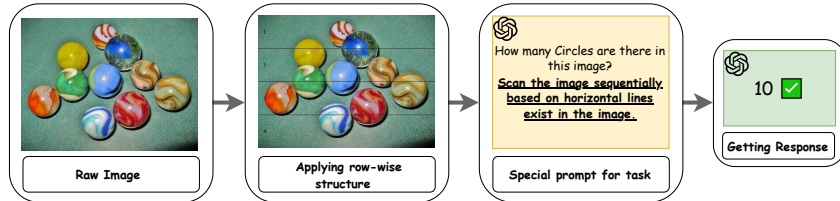


Figure 1: Overview of the proposed method. The input image is augmented with simple spatial scaffolding using 3 horizontal lines to impose a low-level visual structure. A corresponding textual prompt (“*Scan the image sequentially based on horizontal lines*”) is appended to encourage the model to adopt a spatially guided, sequential parsing strategy.

refers to the difficulty of correctly associating visual features (like shape and color) and spatial properties (such as location and orientation) with the right objects in a scene. It arises when a system must handle multiple entities simultaneously, leading to interference and misattribution of features [10–12]. In the context of VLMs, the binding problem manifests as errors in compositional understanding—models may recognize individual objects correctly but confuse or conflate their attributes. These issues are particularly prevalent in complex, cluttered scenes and persist across a range of model architectures and benchmarks. As a result, reliable multi-object reasoning and generalization of visual concepts to novel settings remain difficult for current VLMs.

Inspired by the neuroscientific studies on human scene perception, in this work, we propose a novel approach to improve VLM binding performance. Our approach augments visual inputs with low-level spatial structures, such as horizontal or grid lines, complemented by appending a textual instruction to the input prompt (See Figure 1 as an example). The motivation behind our strategy is to encourage sequential processing in VLMs guided by these interventions in the inputs. Our method can be viewed as a visual analogue of Chain-of-Thought (CoT) prompting[13] for LLMs, as it injects an expert-designed inductive bias directly into the visual input to implicitly decompose the problem and guide the model’s reasoning.

Despite its simplicity, our method yields significant improvements in performance. Moreover, we empirically show that both visual and textual components of our method are necessary and complementary. In particular, textual prompts for sequential scanning alone prove insufficient to resolve binding failures, and even attempts to elicit more structured reasoning through complex prompting strategies, such as Chain-of-Thought (CoT), can paradoxically degrade performance on these visual tasks [14]. In contrast, the inclusion of visual cues stimulates more structured internal processing in VLMs and promotes spatial parsing mechanisms, enhancing the model’s ability to bind features accurately. These findings highlight the potential of targeted visual input modifications to improve graphical reasoning and compositional understanding in VLMs. In summary, the main contributions of this paper are:

- We propose a novel method that combines explicit visual scaffolding (e.g., horizontal lines) with targeted textual prompts to improve feature-object binding in VLMs.
- Through extensive experiments, we demonstrate that our method significantly enhances VLM performance across a range of core visual reasoning tasks, including visual search, counting, scene description, and spatial relationship understanding. For example, on a 2D scene understanding task using GPT-4o, we improve the accuracy of visual search by 25.00%, counting by 26.83%, and spatial relationships by 9.50%, while also reducing the edit distance error for the scene description task by 0.32.
- Our results establish that purely textual interventions are insufficient to overcome binding limitations, and explicit visual manipulation is crucial for this purpose.
- The proposed intervention achieves these improvements efficiently, operating within a single query and incurring negligible computational overhead. This efficiency distinguishes our method from multi-query or existing agentic approaches.

2 Related Work

LLM and VLM Reasoning. While early LLMs were regarded as next-token predictors with little reasoning ability [15, 16], recent work has begun to extensively challenge this problem [17–20].

Today’s state-of-the-art models deliver high performance across many tasks, including graduate-level question answering [21] and competitive programming. The improved reasoning abilities of LLMs have naturally sparked interest in reasoning for VLMs. Initial approaches include Visual Chain-of-Thought [22], knowledge graph integration [23], and tree search [24]. Although these techniques show promise, VLMs still struggle with tasks such as counting, visual search, scene description, and spatial reasoning, as demonstrated by benchmarks like EMMA [14] and SPACE [25]. Our work aims to incorporate an explicit reasoning pathway into the visual component of the model to improve its performance on these challenging tasks.

Binding Problem. The binding problem offers a key explanation for the challenges faced by state-of-the-art VLMs in associating different features of objects, such as shape and location. [26, 27]. Some studies suggest that performance issues in tasks like counting, visual search, and scene description can be attributed to binding problems in models [9]. Recent neuroscience research has shown that grid-based frameworks enhance visual recognition memory [28] and improve face recognition performance [29]. Additionally, humans reduce interference by detecting individual objects iteratively [30, 10], and grid structures facilitate movement-based object recognition [31], thus providing insight into how the human brain can deal with the binding problem. Inspired by these insights, we use horizontal lines in images to enhance model reasoning, both with synthetic images and real-world datasets, such as the Everything Counts benchmark [32].

Agentic VLMs. An emerging line of research treats VLMs as autonomous tool users that can invoke external modules or produce executable artefacts to compensate for perceptual or reasoning gaps. LVLM-COUNT [33] decomposes enumerative queries into sub-counts solved by a specialized counting utility, yielding gains on counting benchmarks. Visual Sketchpad [34] endows multimodal LMs with a drawable canvas, letting them sketch auxiliary lines and marks. Code execution agents such as ViperGPT [35] translate natural-language questions into Python scripts that orchestrates off-the-shelf vision tools, achieving state-of-the-art results on compositional visual queries. While Toolformer [36] shows that language models can self-supervise the decision of when and how to call external APIs. Although these approaches boost task performance, they do not enrich the models’ intrinsic reasoning capabilities. In contrast, our work embeds an explicit reasoning pathway directly into the visual input to overcome these limitations.

3 Proposed Method

The binding problem—a fundamental challenge in cognitive science and neuroscience—concerns how perceptual systems correctly associate features like color, shape, and location with the right objects in complex visual scenes [10, 12]. When multiple objects share representational resources, the system can produce *illusory conjunctions*, i.e., erroneous confusion of features from different objects (e.g., mistakenly perceiving a red square when shown a red circle and a green square) [11]. These misbindings reveal the inherent difficulty of forming coherent, object-specific representations from a distributed set of visual information and analyzing them offers a valuable framework for assessing the capability and reliability of visual reasoning systems across diverse tasks.

Neuroscientific studies show that human visual system operates in two distinct modes: ¹ Parallel processing is fast but imprecise, particularly in cluttered scenes where binding demands are high. When given sufficient time budget, humans perform a more accurate feature binding by transitioning from the parallel analysis to the sequential attention. In contrast, current VLMs process inputs predominantly in parallel. This parallel feature extraction is a double-edged sword; while it enables compositional representation learning—supporting flexibility and generalization—it inherently creates the risk for interference and binding errors, particularly if feature-to-object linkages are not meticulously managed [27].

To address the binding problem in VLMs, we propose a lightweight, model-agnostic approach that enhances structured visual reasoning through minimal visual scaffolding and spatially grounded prompting. Inspired by cognitive science findings on serial attention and spatial structuring, our method guides VLMs to process visual information region-by-region and reduces interference effects from parallel processing, a known contributor to binding errors in human and machine vision. This approach introduces negligible computational overhead, requires no task-specific fine-tuning or

¹Also called *System 1* and *System 2* in the context of visual reasoning [37].

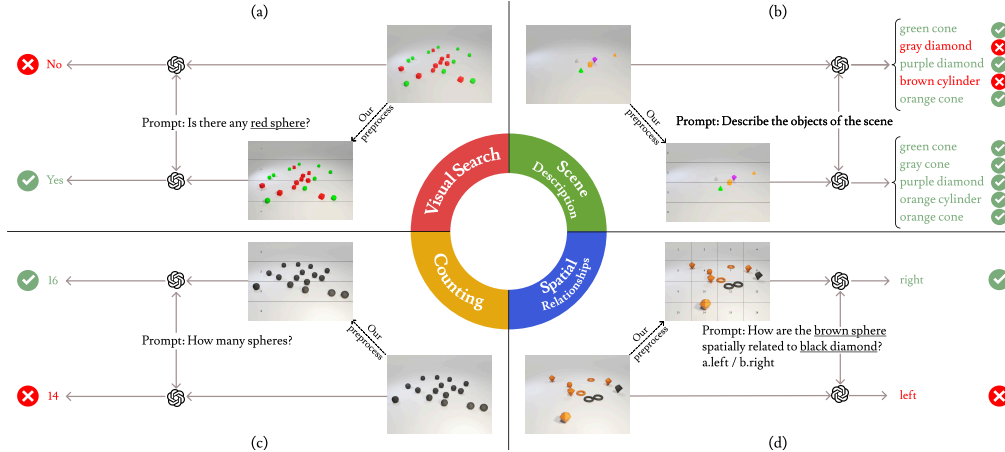


Figure 2: A brief summary of tasks with one example of synthetic data along the specific prompt for each task. (a) Visual Search, (b) Spatial Relationship, (c) Counting, and (d) Spatial Relationship.

multi-query visual processing, and comprises two main components, which are illustrated with an example in Figure 1 and explained below:

Visual Structuring with Horizontal Lines We augment each input image with n equidistant horizontal lines, partitioning it into $n + 1$ segments numbered sequentially from top to bottom (1 through $n + 1$). These lines serve as visual anchors, promoting localized attention within each region to reduce cross-object interference and improve feature-object binding. Unlike dense grid-based methods that may obscure content, our minimalist design preserves clarity while providing sufficient spatial guidance. The value of n is set to 3 in our experiments.

Sequential Scanning Prompt To align the model’s attention with the visual scaffold, we prepend a fixed instruction, specifically: “Scan the image sequentially based on horizontal lines exists in the image.” This prompt guides the model to adopt a structured, row-wise processing strategy, encouraging a systematic evaluation of the image content. For task-specific adaptation (e.g., counting or spatial reasoning), we augment the base prompt with additional instructions (see Appendix D).

The use of manually added artifacts and the emphasis on sequential, region-based processing may also align with the discussion of feature entropy in [9]. By partitioning the image into distinct segments, our method encourages focused processing on smaller subsets of objects. This can simplify the distinction between objects within each segment by reducing the concurrent feature load, an effect pertinent to managing feature diversity (or entropy) as detailed in [9]. Such simplification is a key factor contributing to improved visual reasoning, particularly in counting.

4 Experiments

4.1 Setup

Datasets To evaluate our method, we use both synthetic and natural datasets. A Binding Problem Generator [9] produces synthetic data that can be controlled in two dimensions and three dimensions and can incorporate a variable number of objects. Additionally, we benchmark on two real-world tasks: Learning To Count Everything [32] and the Spatial Reasoning [38] datasets.

Models We evaluated our proposed method across a carefully chosen mix of closed-source and open-source VLMs. Specifically, we include two leading closed-source systems—OpenAI’s GPT-4o [39] and Anthropic’s Claude3.5-sonnet [40]—selected for their cutting-edge capabilities and solid performance on multimodal benchmarks. For GPT-4o, we evaluate both our method and Chain-of-Thought (CoT) prompting [13] to enable a direct comparison within the same architecture. Additionally, we benchmark two state-of-the-art open-source models: Qwen2.5-VL-7B-Instruct [41] and LLaMa4-scout-17b-16e-Instruct [42]. Beyond these baselines, we assess the benefits of targeted fine-tuning by incorporating Mulbary [24], a Qwen2.5VL-7B variant refined for enhanced multimodal reasoning. This breadth of model selection allows us to rigorously assess the generality and robustness of our approach across diverse architectures, training scales, and access constraints.

Table 1: Harmonic mean comparison for the Visual Search task, evaluating our method against base models across GPT-4o, Claude3.5-sonnet, LLaMa4, and Qwen2.5-VL on 2D and 3D datasets with varying numbers of objects.

Dataset	Objects	GPT-4o		Claude-sonnet		LLaMa4		Qwen2.5-VL	
		Simple	Ours	Simple	Ours	Simple	Ours	Simple	Ours
2D	20	0.71	0.91	0.55	0.82	0.00	0.06	0.31	0.43
	30	0.50	0.80	0.54	0.70	0.00	0.00	0.28	0.37
	40	0.25	0.64	0.18	0.59	0.00	0.00	0.14	0.23
	50	0.46	0.55	0.10	0.55	0.00	0.00	0.47	0.56
	Avg	0.48	0.73	0.34	0.66	0.00	0.02	0.30	0.40
3D	20	1.00	1.00	1.00	1.00	0.82	0.80	0.33	0.44
	30	0.96	0.96	0.88	0.91	0.43	0.60	0.15	0.18
	40	0.89	0.94	0.72	0.80	0.59	0.58	0.00	0.15
	50	0.81	0.84	0.59	0.75	0.39	0.38	0.00	0.04
	Avg	0.91	0.93	0.80	0.86	0.56	0.59	0.12	0.20

Evaluation Metrics We use three metrics adopted in visual reasoning research: accuracy, harmonic mean, and edit distance. Accuracy, used for counting and spatial relationship tasks [14], measures the proportion of correct predictions. Harmonic mean evaluates visual search by balancing performance across visible and invisible object detection [9], ensuring that high scores require consistent performance on both subtasks. Edit distance (Levenshtein distance) computes the minimum number of insertions, deletions, or substitutions needed to transform a model-generated scene description into the reference [9], offering a fine-grained measure of binding precision in generated text.

In addition to the main experiments reported in the following subsections, a set of ablation studies is provided in Appendix A.

4.2 Visual Search

Visual search task challenges models to locate a target object among distractors, with task difficulty adjusted by the similarity between target and distractor features. In conjunctive search, where the target is defined by a unique combination of features (e.g., a green L-shape) and distractors partially share these features (e.g., red L-shapes, green T-shapes), successful identification depends on accurate feature binding. Models that struggle with binding may exhibit degraded performance as the number of distractors increases or when features are highly confusable, mirroring human performance limitations when serial attentional scanning is prevented [10].

An instance of the visual search problem is presented in Figure 2-(a); to evaluate our method, we use the synthetic dataset described earlier to generate 2D and 3D scenes containing between 20 and 50 objects of varying complexities. We assessed performance by measuring accuracy in correctly identifying the target’s presence or absence, distinguishing between “visible” searches (the object is explicitly in the scene) and “invisible” searches (the object is absent). This distinction is important because simpler visual-language models often default to predicting “false,” inflating their invisible-object accuracy while failing to detect visible targets. After computing the accuracy for visible and invisible subtasks, we combined them via the harmonic mean to produce a final score.

$$\text{Harmonic Mean} = \frac{2 \cdot \text{Visible} \cdot \text{Invisible}}{\text{Visible} + \text{Invisible}} \quad (1)$$

Table 1 compares our approach against baselines, showing our method delivers consistent and substantial gains over the simple baseline across 2D and 3D scenes and for all evaluated VLMs. In 2D settings, the average harmonic mean for GPT-4o climbs from 0.48 to 0.73, for Claude3.5-sonnet from 0.34 to 0.66, for LLaMa4 from 0.00 to 0.02, and for Qwen2.5-VL from 0.30 to 0.40, with the largest relative improvements occurring as scene complexity increases (e.g., at 40 objects GPT-4o rises from 0.25 to 0.64, and Claude3.5-sonnet rises from 0.18 to 0.59). In 3D scenes our method still yields gains to 0.93, and weaker models benefit notably (Claude3.5-sonnet: 0.80 \rightarrow 0.86; LLaMa4:

Table 2: Performance comparison on the counting task using models GPT-4o, Claude3.5-sonnet, LLaMa4, and Qwen2.5-VL, evaluated with accuracy (%) . The comparison is conducted across 2D and 3D datasets with varying numbers of objects in the scene, as well as a natural image dataset. Results are shown for base models and our method.

Dataset	Objects	GPT-4o		Claude-sonnet		LLaMa4		Qwen2.5-VL	
		Simple	Ours	Simple	Ours	Simple	Ours	Simple	Ours
2D	10	42.00	65.00	26.00	26.00	23.00	31.00	18.00	41.00
	12	12.00	40.00	5.00	15.00	3.00	20.62	1.00	45.00
	14	1.00	34.00	5.00	9.00	0.00	23.47	1.00	13.00
	16	3.00	39.00	3.00	6.00	11.00	23.00	1.00	59.00
	18	1.00	29.00	6.00	4.00	0.00	9.28	0.00	10.00
	20	13.00	26.00	6.00	4.00	1.00	7.22	14.00	77.00
	Avg		12.00	38.83	8.50	10.67	6.33	19.10	5.83
3D	10	52.00	62.00	56.00	54.00	32.00	60.42	20.83	66.00
	12	12.00	38.00	26.00	28.00	0.00	34.69	8.16	20.00
	14	6.00	14.00	14.00	24.00	12.00	38.00	4.08	24.00
	16	16.00	24.00	8.00	14.00	40.00	44.00	6.00	16.00
	18	2.00	18.00	0.00	8.00	0.00	18.75	0.00	14.00
	20	2.00	30.00	0.00	4.00	0.00	22.45	12.00	20.00
	Avg		15.00	31.00	17.33	22.00	14.00	36.39	8.51
Natural		29.82	35.65	2.09	6.42	29.22	31.65	18.91	17.29

0.56 \rightarrow 0.59; Qwen2.5-VL: 0.12 \rightarrow 0.20). These results confirm that our strategy not only corrects the “always-false” bias of simpler VLMs in invisible-object tasks but also markedly enhances their ability to detect visible targets, achieving robust performance regardless of object count, visibility, or scene dimensionality.

4.3 Counting

Counting involves determining the number of specific objects within a scene. Although it may appear simple, accurate enumeration—especially when multiple object types or attribute variations are involved—relies heavily on effective feature binding. Each object must be individuated, its defining features correctly associated, and then counted as a distinct instance. Failures in binding can lead to omissions, double-counting, or misclassification. Similar to human rapid estimation under time constraints, VLMs show capacity limits in counting. Performance often worsens as object numbers grow, or when high object similarity (low feature heterogeneity) increases the interference and binding errors.

An instance of this task is demonstrated in Figure 2-(c); To evaluate our method, we generated 2D and 3D images, using the synthetic data set described above, each containing between 10 and 20 instances of the target object to increase complexity. We measure performance using counting accuracy; the results are summarized in Table 2. As presented, our counting-specific prompting yields substantial gains on synthetic benchmarks: in 2D scenes, GPT-4o jumps from 12.0% to 38.8%, Claude-sonnet from 8.5% to 10.67%, LLaMa4 from 6.3% to 19.1%, and Qwen2.5-VL surges from 5.8% to 40.8%; in 3D scenes, GPT-4o climbs from 15.0% to 31.0%, Claude-sonnet from 17.3% to 22.2%, LLaMa4 from 14.0% to 36.4%, and Qwen2.5-VL from 8.5% to 26.7%. On natural images, improvements are more modest—GPT-4o from 29.8% to 35.7%, Claude-sonnet from 2.09% to 6.4%, LLaMa4 from 29.2% to 31.7%—and Qwen2.5-VL sees a slight drop (18.9% to 17.3%). These results underscore the effectiveness of task-aware prompting in controlled settings while highlighting the remaining challenge of generalizing to real-world imagery.

4.4 Scene Description

The scene description task requires models to generate accurate textual narratives that describe the objects, their attributes, and their relationships within an image. This task challenges a VLM’s ability

Table 3: Comparison of scene description performance (lower is better; measured as average distance) for our method versus base models and CoT prompting across GPT-4o and Claude3.5-sonnet on 2D and 3D datasets with varying numbers of objects.

Dataset	Objects	GPT-4o		Claude-sonnet		LLaMa4		Qwen2.5-VL	
		Simple	Ours	Simple	Ours	Simple	Ours	Simple	Ours
2D	10	0.70	0.67	4.68	3.12	2.03	2.29	4.38	4.24
	15	1.79	1.48	2.89	2.24	3.19	3.99	7.71	7.35
	20	3.32	2.73	1.45	1.24	5.74	6.89	12.29	10.59
	Avg	1.94	1.62	3.01	2.20	3.65	4.39	8.12	7.39
3D	10	4.06	4.25	5.40	5.18	5.04	5.55	7.88	6.61
	15	7.29	7.48	8.56	7.95	9.39	10.60	11.56	10.69
	20	12.38	12.21	14.37	12.03	14.90	16.45	15.84	15.24
	Avg	7.91	7.98	9.45	8.39	9.78	10.84	11.76	10.84

Table 4: Accuracy (%) comparison of spatial relationship predictions across GPT-4o, Claude3.5-sonnet, LLaMa4, and Qwen2.5-VL on 2D, and natural image datasets using base models, CoT prompting, and our method.

	GPT-4o		Claude-sonnet		LLaMa4		Qwen2.5-VL	
	Simple	Ours	Simple	Ours	Simple	Ours	Simple	Ours
2D	43.00	52.50	34.18	36.26	29.50	27.50	48.50	50.00
3D	64.00	68.50	72.50	76.50	55.00	58.50	78.00	82.50
Natural	69.39	77.43	37.43	46.15	58.67	66.84	80.10	77.04

to solve the binding problem. The model must not only detect features (e.g., “red”, “cube”, “blue”, “sphere”) but also correctly associate them with the corresponding objects in its textual output (e.g., “a red cube and a blue sphere”, not “a blue cube and a red sphere”). Errors, such as attribute swapping or incorrectly pairing features with objects, often arise in complex scenes. This typically occurs when multiple objects share some features but differ in others, which inherently challenges precise feature-object binding.

Figure 2-(b) shows an instance of the scene description task; we evaluate a synthetically generated dataset of 2D and 3D scenes, each containing between 10 and 20 objects to vary scene complexity. Model performance is quantified by the edit distance between the generated descriptions and the ground-truth annotations; we show more detail about this in Appendix C. This yields three outcome categories: (1) an exact match, (2) a single-attribute mismatch (either shape or color), and (3) a double-attribute mismatch (both shape and color). The full results are presented in Table 3. The greatest average gains (-0.81 in 2D and -1.06 in 3D) are driven precisely where the task’s difficulty peaks, showing that the technique not only endures extra clutter but thrives on it. This confirms that our method is the most reliable option for reasoning with a high object count.

4.5 Spatial Relationship

In this task, the model is expected to identify and verify the relative positions of objects in a scene (e.g., “Is the red cube to the left of the blue sphere?”). This involves not only correctly binding intrinsic features (e.g., color, shape) to objects but also accurately associating each object with its spatial location, followed by a relational comparison. Failure to bind features properly can lead to misidentification of the objects being queried. Furthermore, if the VLM cannot accurately associate each identified object with its precise location, its capacity to reason about their relative positions will be compromised. VLMs often struggle with spatial reasoning due to their inability to maintain distinct, spatially grounded representations of multiple objects simultaneously [8].

An example of the spatial relationship task is presented in Figure 2-(d); To evaluate our method, we generated 2D scenes using the synthetic dataset described earlier and posed four-option multiple-

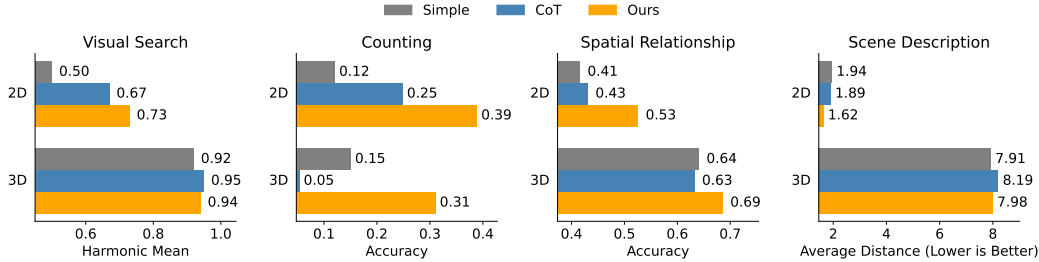


Figure 3: Comparison of our method with Chain-of-Thought (CoT) prompting on the GPT-4o model across four tasks. Each subplot shows the performance of three methods—Simple (base), CoT, and Ours (our method)—evaluated using a task-specific metric indicated on the x-axis. Bars are grouped into 2D and 3D datasets.

choice questions for each scene, asking models to select the answer that best describes the spatial relation between the target objects. The evaluation results are shown in Table 4. As you can see, the new results show that our method (“Ours” column) yields consistent gains for most models: GPT-4o rises from 43.00% to 52.50% (+9.50%) on 2D, 64.00% to 68.50% (+4.50%) on 3D, and 69.39% to 77.43% (+8.04%) on natural scenes; Claude-sonnet jumps from 34.18% to 36.26% (+2.08%) on 2D, 72.50% to 76.50% (+4.00%) on 3D, and 37.43% to 46.15% (+8.72%) on natural images; LLaMa4 dips 2.00% on 2D but improves 3.50% on 3D and 8.17% on natural; and Qwen2.5-VL gains 1.50% on 2D and 4.5% on 3D yet sees a 3.06% drop on natural scenes. Overall, our approach particularly enhances 3D spatial reasoning—most dramatically for Claude-sonnet—and substantially boosts real-image performance in large models, while smaller or vision-augmented models show more mixed effects on natural data.

4.6 Chain of Thought

To examine whether purely textual reasoning cues can bridge the binding gap, we pit our visually structured prompt against a Chain-of-Thought (CoT) baseline. The baseline employs GPT-4o with the canonical cue “Let’s think step by step” [13] appended to each instruction, leaving the image untouched, mirroring standard practice for eliciting step-wise reasoning in language models. Across all four tasks, our method consistently surpasses both the Simple model (no reasoning prompt) and the CoT variant in 2D and 3D scenarios (Figure 3). Crucially, the gap is far more pronounced on the 2D datasets. Flattened scenes crowd objects into a single plane, intensifying cross-object interference and making accurate binding harder. In these cluttered 2D settings, the lightweight spatial scaffold provides the model with an external, row-by-row traversal plan, producing markedly larger gains than CoT; in 3D scenes, the relative advantage narrows but persists. These results underline that verbal reasoning alone is not enough. A CoT prompt can encourage the model to explain its answer, but it cannot repair a noisy, globally pooled image embedding. Once early tokens are conditioned on entangled visual features, every subsequent “step” inherits the same misbindings. The scaffold, by contrast, prestructures the visual input so that each attended region contains fewer competing objects, allowing the language model to reason over cleaner, localized representations. Thus, reliable multimodal reasoning emerges only when textual chains of thought are paired with a minimal but crucial spatial guide.

4.7 Fine-Tuning for Visual Reasoning

To evaluate whether our lightweight method can match the benefits of model-level adaptation, we compare it to Mulberry [24], a Qwen2.5-VL variant fine-tuned for visual reasoning. As shown in Figure 4, we evaluate the base Qwen2.5-VL model, our method, and the fine-tuned Mulberry model across all tasks. Our method consistently improves over the base model and often matches or outperforms Mulberry, despite requiring no fine-tuning or access to model internals. For example, in 2D counting, Qwen-Ours reaches 41% accuracy, surpassing Mulberry’s 15%. These results show that addressing the binding problem through simple visual scaffolding and spatial prompting, without additional supervision or computational cost, can be as effective as training-based approaches for enhancing visual reasoning.

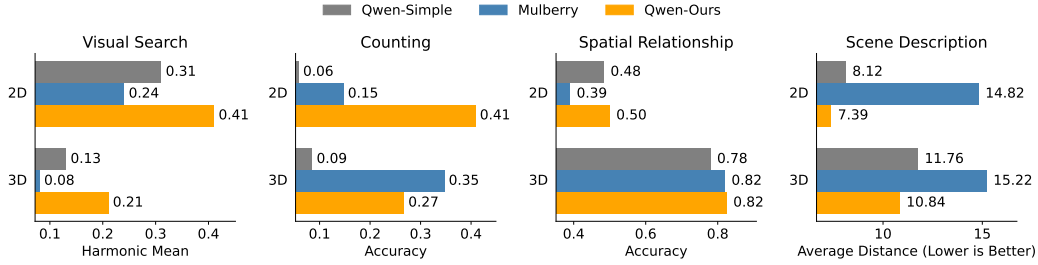


Figure 4: Comparison of our method with visual reasoning–finetuned model on the Qwen2.5-VL base model across four tasks. Each subplot shows the performance of three methods—Qwen-Simple (Qwen2.5-VL), Qwen-Ours (our method applied to Qwen2.5-VL), and Mulberry (Qwen2.5-VL finetuned for visual reasoning)—evaluated using a task-specific metric indicated on the x-axis. Bars are grouped into 2D and 3D datasets.

5 Discussion

This research investigated the binding problem in VLMs, a key factor limiting their performance on structured visual reasoning tasks. We introduced a method combining simple visual scaffolding, using horizontal lines, with a targeted textual prompt to encourage sequential, spatially-aware processing. Our experiments demonstrate that this intervention leads to substantial and consistent performance improvements across visual search, counting, scene description, and spatial relationship understanding. These results support the hypothesis that explicit low-level visual structure improves feature-object binding.

A central finding is the critical role of visual structures. While textual prompts alone proved insufficient and sometimes detrimental, the addition of visual lines significantly improved reasoning accuracy. This suggests that current VLMs, despite their advanced linguistic capabilities, can benefit greatly from external visual cues that facilitate a more systematic parsing of complex scenes. The visual scaffolding appears to help models approximate a serial attentional process, mitigating the interference and illusory conjunctions when processing multiple objects and their features in parallel. This localized, sequential processing may also reduce representational interference by effectively managing feature entropy within sub-regions of the image, a factor highlighted in [9] as critical for robust visual reasoning. This supports the idea that addressing the binding problem may require interventions at the level of visual input processing, rather than relying solely on linguistic instruction.

The proposed method offers a practical and efficient intervention, readily applicable due to its simplicity, negligible computational overhead, and single-query operation, without reliance on external tools, model fine-tuning, or architectural changes. This highlights visual input structuring as a key strategy for enhancing VLM reasoning, beyond linguistic instruction. While effective, the current static nature of the visual scaffolding represents a potential area for refinement. Future research could investigate adaptive visual scaffolding, where cues are dynamically determined by image content or query specifics. Moreover, developing VLM architectures that inherently support serial, spatially grounded attention, perhaps inspired by these findings, could offer more integrated and robust solutions to the binding problem.

Last but not the least, we emphasize that improved visual reasoning in AI systems can benefit a wide range of applications, from assistive technologies and robotics to education and healthcare. However, as VLMs become more capable, their potential misuse—for instance, in surveillance, automated decision-making, or misinformation—also grows. Our approach does not require model retraining, making it widely accessible, but this also implies that such modifications could be adversarially deployed in black-box systems without transparency or oversight. To mitigate risks, we advocate for responsible use of these techniques in alignment with accountability and transparency guidelines. Moreover, future research should profoundly study the unintended biases that scaffolding might introduce in tasks other than spatial reasoning, especially when used in safety-critical applications.

References

- [1] Trieu H Trinh, Yuhuai Wu, Quoc V Le, He He, and Thang Luong. Solving olympiad geometry without human demonstrations. *Nature*, 625(7995):476–482, 2024.
- [2] Xiaoliang Luo, Akilles Rechartd, Guangzhi Sun, Kevin K Nejad, Felipe Yáñez, Bati Yilmaz, Kangjoo Lee, Alexandra O Cohen, Valentina Borghesani, Anton Pashkov, et al. Large language models surpass human experts in predicting neuroscience results. *Nature human behaviour*, 9(2):305–315, 2025.
- [3] Alejandro Lopez-Lira and Yuehua Tang. Can chatgpt forecast stock price movements? return predictability and large language models. *arXiv preprint arXiv:2304.07619*, 2023.
- [4] Alex Kim, Maximilian Muhn, and Valeri Nikolaev. Financial statement analysis with large language models. *arXiv preprint arXiv:2407.17866*, 2024.
- [5] Michal Kosinski. Evaluating large language models in theory of mind tasks. *Proceedings of the National Academy of Sciences*, 121(45):e2405460121, 2024.
- [6] Jiayu Wang, Yifei Ming, Zhenmei Shi, Vibhav Vineet, Xin Wang, Sharon Li, and Neel Joshi. Is a picture worth a thousand words? delving into spatial reasoning for vision language models. *Advances in Neural Information Processing Systems*, 37:75392–75421, 2024.
- [7] Pooyan Rahmzadehgervi, Logan Bolton, Mohammad Reza Taesiri, and Anh Totti Nguyen. Vision language models are blind. In *Proceedings of the Asian Conference on Computer Vision*, pages 18–34, 2024.
- [8] Amita Kamath, Jack Hessel, and Kai-Wei Chang. What’s "up" with vision-language models? investigating their struggle with spatial reasoning. *arXiv preprint arXiv:2310.19785*, 2023.
- [9] Declan Campbell, Sunayana Rane, Tyler Giallanza, Camillo Nicolò De Sabbata, Kia Ghods, Amogh Joshi, Alexander Ku, Steven Frankland, Tom Griffiths, Jonathan D Cohen, et al. Understanding the limits of vision language models through the lens of the binding problem. *Advances in Neural Information Processing Systems*, 37:113436–113460, 2024.
- [10] Anne M Treisman and Garry Gelade. A feature-integration theory of attention. *Cognitive psychology*, 12(1):97–136, 1980.
- [11] Anne Treisman and Hilary Schmidt. Illusory conjunctions in the perception of objects. *Cognitive psychology*, 14(1):107–141, 1982.
- [12] Adina L Roskies. The binding problem. *Neuron*, 24(1):7–9, 1999.
- [13] Takeshi Kojima, Shixiang Shane Gu, Machel Reid, Yutaka Matsuo, and Yusuke Iwasawa. Large language models are zero-shot reasoners. *Advances in neural information processing systems*, 35:22199–22213, 2022.
- [14] Yunzhuo Hao, Jiawei Gu, Huichen Will Wang, Linjie Li, Zhengyuan Yang, Lijuan Wang, and Yu Cheng. Can mllms reason in multimodality? emma: An enhanced multimodal reasoning benchmark. *arXiv preprint arXiv:2501.05444*, 2025.
- [15] Jie Huang and Kevin Chen-Chuan Chang. Towards reasoning in large language models: A survey. *arXiv preprint arXiv:2212.10403*, 2022.
- [16] Jie Huang, Xinyun Chen, Swaroop Mishra, Huaixiu Steven Zheng, Adams Wei Yu, Xinying Song, and Denny Zhou. Large language models cannot self-correct reasoning yet. *arXiv preprint arXiv:2310.01798*, 2023.
- [17] Yu Zhao, Huifeng Yin, Bo Zeng, Hao Wang, Tianqi Shi, Chenyang Lyu, Longyue Wang, Weihua Luo, and Kaifu Zhang. Marco-o1: Towards open reasoning models for open-ended solutions. *arXiv preprint arXiv:2411.14405*, 2024.
- [18] OpenAI. Learning to Reason with LLMs. <https://openai.com/index/learning-to-reason-with-llms/>, September 2024. Accessed: 2025-05-15.

- [19] Qwen Team. QwQ: Reflect deeply on the boundaries of the unknown. <https://qwenlm.github.io/blog/qwq-32b-preview/>, November 2024. Accessed: 2025-05-15.
- [20] Wenfeng Liang, Zehui Ren, Zhangli Sha, Zhe Fu, Zhean Xu, Zhenda Xie, Zhengyan Zhang, Zhewen Hao, Zhicheng Ma, Zhigang Yan, Zhiyu Wu, Zihui Gu, Zijia Zhu, Zijun Liu, Zilin Li, Ziwei Xie, Ziyang Song, Zizheng Pan, Zhen Huang, Zhipeng Xu, Zhongyu Zhang, Zhen Zhang, and et al. Deepseek-r1: Incentivizing reasoning capability in llms via reinforcement learning. *arXiv preprint arXiv:2501.12948*, 2025. doi: 10.48550/arXiv.2501.12948. URL <https://arxiv.org/abs/2501.12948>. Accessed: 2025-05-15.
- [21] David Rein, Betty Li Hou, Asa Cooper Stickland, Jackson Petty, Richard Yuanzhe Pang, Julien Dirani, Julian Michael, and Samuel R Bowman. Gpqa: A graduate-level google-proof q&a benchmark. In *First Conference on Language Modeling*, 2024.
- [22] Hao Shao, Shengju Qian, Han Xiao, Guanglu Song, Zhuofan Zong, Letian Wang, Yu Liu, and Hongsheng Li. Visual cot: Advancing multi-modal language models with a comprehensive dataset and benchmark for chain-of-thought reasoning. *Advances in Neural Information Processing Systems*, 37:8612–8642, 2024.
- [23] Yichi Zhang, Zhuo Chen, Lingbing Guo, Yajing Xu, Binbin Hu, Ziqi Liu, Wen Zhang, and Huajun Chen. Native: Multi-modal knowledge graph completion in the wild. In *Proceedings of the 47th International ACM SIGIR Conference on Research and Development in Information Retrieval*, pages 91–101, 2024.
- [24] Huanjin Yao, Jiaying Huang, Wenhao Wu, Jingyi Zhang, Yibo Wang, Shunyu Liu, Yingjie Wang, Yuxin Song, Haocheng Feng, Li Shen, et al. Mulberry: Empowering mllm with o1-like reasoning and reflection via collective monte carlo tree search. *arXiv preprint arXiv:2412.18319*, 2024.
- [25] Santhosh Kumar Ramakrishnan, Erik Wijmans, Philipp Kraehenbuehl, and Vladlen Koltun. Does spatial cognition emerge in frontier models? *arXiv preprint arXiv:2410.06468*, 2024.
- [26] C. Von Der Malsburg. The correlation theory of brain function. in models of neural networks: Temporal aspects of coding and information processing in biological systems. *Neuron*, pages 95—119, 1994.
- [27] Klaus Greff, Sjoerd Van Steenkiste, and Jürgen Schmidhuber. On the binding problem in artificial neural networks. *arXiv preprint arXiv:2012.05208*, 2020.
- [28] Andrej Bicanski and Neil Burgess. A computational model of visual recognition memory via grid cells. *Current Biology*, 29(6):979–990, 2019.
- [29] Jie Liu, Wenqiang Xu, Xiumin Li, and Xiao Zheng. Improved visual recognition memory model based on grid cells for face recognition. *Frontiers in Neuroscience*, 15:718541, 2021.
- [30] Pieter R Roelfsema. Solving the binding problem: Assemblies form when neurons enhance their firing rate—they don’t need to oscillate or synchronize. *Neuron*, 111(7):1003–1019, 2023.
- [31] Niels Leadholm, Marcus Lewis, and Subutai Ahmad. Grid cell path integration for movement-based visual object recognition. *arXiv preprint arXiv:2102.09076*, 2021.
- [32] Viresh Ranjan, Udbhav Sharma, Thu Nguyen, and Minh Hoai. Learning to count everything. In *Proceedings of the IEEE/CVF Conference on Computer Vision and Pattern Recognition*, pages 3394–3403, 2021.
- [33] Muhammad Fetrat Qharabagh, Mohammadreza Ghofrani, and Kimon Fountoulakis. Lvlm-count: Enhancing the counting ability of large vision-language models. *arXiv preprint arXiv:2412.00686*, 2024.
- [34] Yushi Hu, Weijia Shi, Xingyu Fu, Dan Roth, Mari Ostendorf, Luke Zettlemoyer, Noah A Smith, and Ranjay Krishna. Visual sketchpad: Sketching as a visual chain of thought for multimodal language models. *arXiv preprint arXiv:2406.09403*, 2024.

- [35] Dídac Surís, Sachit Menon, and Carl Vondrick. Vipergpt: Visual inference via python execution for reasoning. In *Proceedings of the IEEE/CVF International Conference on Computer Vision*, pages 11888–11898, 2023.
- [36] Timo Schick, Jane Dwivedi-Yu, Roberto Dessì, Roberta Raileanu, Maria Lomeli, Eric Hambro, Luke Zettlemoyer, Nicola Cancedda, and Thomas Scialom. Toolformer: Language models can teach themselves to use tools. *Advances in Neural Information Processing Systems*, 36: 68539–68551, 2023.
- [37] Sang C Chong and Karla K Evans. Distributed versus focused attention (count vs estimate). *Wiley Interdisciplinary Reviews: Cognitive Science*, 2(6):634–638, 2011.
- [38] Fatemeh Shiri, Xiao-Yu Guo, Mona Golestan Far, Xin Yu, Gholamreza Haffari, and Yuan-Fang Li. An empirical analysis on spatial reasoning capabilities of large multimodal models. *arXiv preprint arXiv:2411.06048*, 2024.
- [39] OpenAI. GPT-4o: A multimodal large language model. <https://openai.com/product/gpt-4o>, 2024.
- [40] Anthropic. Claude 3.5 Sonnet: Mid-tier intelligence with advanced reasoning. <https://www.anthropic.com/news/claude-3-5-sonnet>, June 2024. Accessed: 2025-05-11.
- [41] Bai, Shuai and Chen, Keqin and Liu, Xuejing and Wang, Jialin and Ge, Wenbin and Song, Sibao and Dang, Kai and Wang, Peng and Wang, Shijie and Tang, Jun and Zhong, Humen and Zhu, Yuanzhi and Yang, Mingkun and Li, Zhaohai and Wan, Jianqiang and Wang, Pengfei and Ding, Wei and Fu, Zheren and Xu, Yiheng and Ye, Jiabo and Zhang, Xi and Xie, Tianbao and Cheng, Zesen and Zhang, Hang and Yang, Zhibo and Xu, Haiyang and Lin, Junyang et al. Qwen2.5-VL: Technical report. *arXiv preprint arXiv:2502.13923*, 2025. Accessed: 2025-05-14.
- [42] Meta AI. LLaMA 4: Natively multimodal large language model family. <https://ai.meta.com/blog/llama-4-multimodal-intelligence/>, 2025.
- [43] Yihe Deng, Hritik Bansal, Fan Yin, Nanyun Peng, Wei Wang, and Kai-Wei Chang. Openvlthinker: An early exploration to complex vision-language reasoning via iterative self-improvement, 2025. URL <https://arxiv.org/abs/2503.17352>.

Table 5: Comparison of our method and other ablation methods on GPT-4o in 2D scenes across multiple tasks.

Method	Scene Desc. (Edit Dist.)	Counting (Accuracy)	Visual Search (Accuracy)
Simple	1.81	16.85	0.48
Ours	1.61	31.55	0.73
Ours–NoRowNum	1.71	19.14	0.70
Column	2.00	16.68	0.76
Grid	2.43	17.40	0.72

A Ablation study

In our ablation study, we assess multiple scene-structuring strategies and their impact on task performance using the GPT-4o [39] model. All experiments are conducted on a consistent subset of our 2D synthetic dataset [9], with varying object counts per scene. The results in Table 5 show the average performance across these scenes.

The Simple setting represents the baseline configuration, where the model is prompted to describe the image without any additional structuring cues. As shown, this baseline yields the lowest or near the lowest accuracy in counting and visual search, indicating that unstructured prompts are insufficient for supporting systematic reasoning.

Among the structured variants, the Grid-based layout consistently performs the worst, particularly in the scene description task, likely due to excessive spatial fragmentation hindering its interpretation of coherent groupings. The Column-based layout also underperforms in both scene description and counting tasks compared to horizontal-based layouts, suggesting that vertical splitting is suboptimal for global scene comprehension. Interestingly, it achieves a small gain in visual search, where object-level localization is more critical than spatial integration.

In contrast, our row-based horizontal structuring, which explicitly divides the image into horizontal bands, leads to improved performance across all tasks. This design encourages the model to scan the scene in a consistent, line-by-line fashion. Furthermore, removing numerical indices from rows (Ours–NoRowNum) results in a substantial drop in accuracy, highlighting the value of explicit ordering cues in guiding sequential attention.

These results collectively underscore the importance of structured, order-aware visual annotations in enabling VLMs to reason more effectively over complex spatial arrangements.

A.1 Reasoning trace evaluation

To evaluate the impact of visual structure on step-by-step reasoning, we compare two prompting strategies for the 2D scene description task. In the first setting, we provide GPT-4o with the original image *without any row markings* and use a prompt that instructs: “*Divide the image into 4 equal horizontal sections from top to bottom, and list the shape and color of each object in each row.*” In the second setting, we explicitly modify the image to include *four horizontal lines* that visually segment the scene into rows. As shown in Figure 5, this structural addition significantly improves performance across all three evaluation metrics (F1 score, Jaccard similarity, and Edit distance) on scenes with 10, 15, and 20 objects. These results suggest that textual instructions alone are insufficient: incorporating structural cues directly into the visual input helps the model follow the intended sequential scanning process more accurately. For consistency, all objects in the scenes were rendered as *colored squares*, and in cases where a square overlapped multiple rows, it was assigned to the row containing the majority of its area. This assignment policy was also reflected explicitly in the prompt.

B Comparison with RL-finetuned Model

We conduct a comprehensive comparison with OpenVLThinker [43], which enhances Qwen2.5-VL through an iterative training pipeline combining supervised finetuning (SFT) and reinforcement learning (RL) to strengthen multimodal reasoning. In contrast, our method requires no post-training phase and operates entirely during inference, yet achieves superior performance across most evaluated tasks. As demonstrated in Figure 6, our approach consistently outperforms both the baseline Qwen2.5-

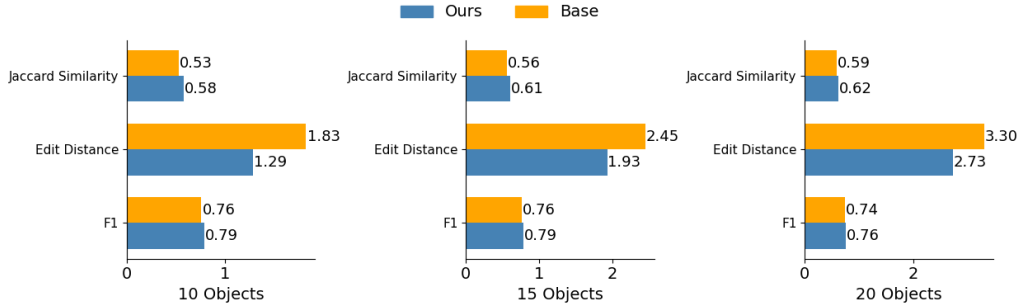


Figure 5: Comparison between our method and GPT-4o in the 2D scene description task, where models sequentially scan the image row by row to identify objects. Results are reported for scenes with 10, 15, and 20 objects using three evaluation metrics: F1 score, Jaccard similarity, and Edit distance.

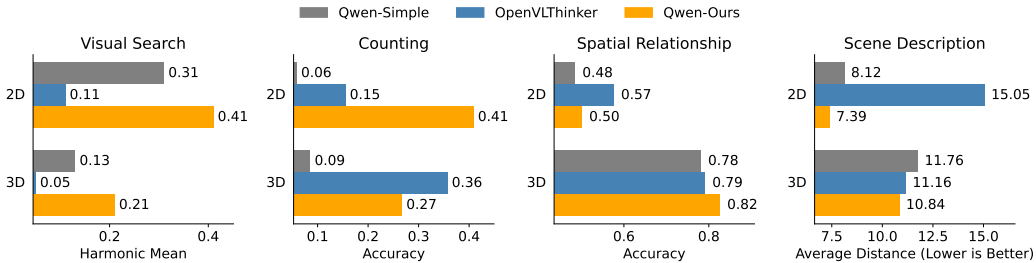


Figure 6: Comparison of our method with a finetuned visual reasoning model on Qwen2.5-VL as the base model across four tasks. Each subplot shows the performance of three methods—Qwen-Simple (Qwen2.5-VL), Qwen-Ours (our method applied to Qwen2.5-VL), and OpenVLThinker (Qwen2.5-VL finetuned with RL-based reasoning)—evaluated using a task-specific metric indicated on the x-axis. Bars are grouped into 2D and 3D datasets for each task.

VL and OpenVLThinker in most reasoning tasks, with particularly significant gains of up to 26% on 2D-Counting task. The only exceptions where OpenVLThinker shows an advantage are in 2D-Spatial reasoning and 3D-Counting tasks, a likely consequence of its RL-based optimization for multimodal reasoning. This suggests that while training-intensive methods can excel in specific domains, they come with substantial computational costs. Our training-free paradigm, by contrast, maintains broader dominance across diverse multimodal reasoning tasks while offering superior scalability and efficiency.

C Benchmark and score details

C.1 Benchmarks

In this study, we introduce a series of benchmarks designed to evaluate the performance of VLMs on various visual reasoning tasks, including visual search, counting, scene description, and spatial reasoning. Each benchmark was specifically developed to provide rigorous and systematic assessments of different VLM capabilities, utilizing both synthetic and real-world data. These benchmarks are structured to facilitate controlled experiments while maintaining diversity in task difficulty, scene configurations, and object arrangements. Below, we provide detailed descriptions of each benchmark used in our evaluation.

C.1.1 Visual Search Benchmark

Building on the same synthetic generation framework from [9], we adapted the pipeline with task-specific configurations for visual search evaluation.

2D Scenes: We created scenes containing 20, 30, 40, and 50 objects. Each configuration comprised 100 images (50 with targets present and 50 absent), totaling 400 2D scenes.

3D Scenes: Using the same object count progression, we generated 50 images per count (25 with targets present and 25 absent), resulting in 200 3D scenes. The reduced quantity accounts for the higher rendering complexity.

Natural image datasets are not suitable for this evaluation, as they lack two critical properties: (1) the ability to systematically adjust distractor characteristics (shape, color, and spatial arrangement) and (2) precise control over target-distractor similarity levels. Our synthetic paradigm provides this essential controllability, allowing a rigorous assessment of binding capabilities through progressive difficulty scaling while maintaining a balanced presence/absence of the target (50% distribution).

C.1.2 Counting Benchmark

To assess the counting ability of VLMs, we developed a comprehensive benchmark based on the generation methodology outlined in [9].

2D Scenes: We generated synthetic 2D scenes with object counts ranging from 10 to 20, incremented in steps of 2 (10, 12, 14, 16, 18, 20). For each object count, we produced 100 distinct images, resulting in a total of 600 2D images.

3D Scenes: Similarly, we created 3D scenes with object counts following the same progression (10 to 20, step size = 2). We generated 50 images per object count, yielding a total of 300 3D images.

To assess real-world generalizability, we incorporated the “Learning to Count Everything” benchmark [32]. We used approximately 300 images containing up to 20 objects to maintain reasonable task difficulty.

This structured approach enables a rigorous assessment of counting performance in controlled synthetic and real-world scenes.

C.1.3 Scene Description Benchmark

Following [9], we define a *feature triplet* as any set of three objects where one pair shares a feature (e.g., color) and another pair shares a different feature (e.g., shape). For example: green X, green triangle, yellow triangle forms a triplet through shared “green” and “triangle” features.

To evaluate scene description capabilities in VLMs, we developed a comprehensive benchmark using the feature triplet methodology from [9] with controlled object counts and systematically varied triplet configurations.

2D Scenes: We generated synthetic 2D scenes with 10, 15, and 20 objects. For 10 objects, we created configurations with 5 to 20 triplets in increments of 5 (5, 10, 15, 20 triplets). For 15 objects, we extended the triplet counts up to 50 (in steps of 5), and for 20 objects up to 70 triplets (also in steps of 5), with 50 images generated for each configuration.

3D Scenes: Following the same progression, we created 3D scenes with identical objects and triplet counts, generating 30 images per triplet count to account for rendering complexity.

The increasing number of feature triplets introduces progressively greater interference among object features, making the binding problem more challenging and testing the model’s reasoning capabilities under increasingly difficult conditions.

This approach enables systematic assessment of scene description performance across: (1) controlled object counts, (2) graduated levels of feature interference through triplet counts, and (3) both 2D and 3D representations. The detailed results for 10, 15, and 20 objects and triplet configurations are presented in Figures 7, 8, and 9, respectively.

C.1.4 Spatial Relationship Benchmark

To evaluate spatial reasoning in VLMs, we developed a comprehensive benchmark using the generation methodology from [9] complemented by natural images.

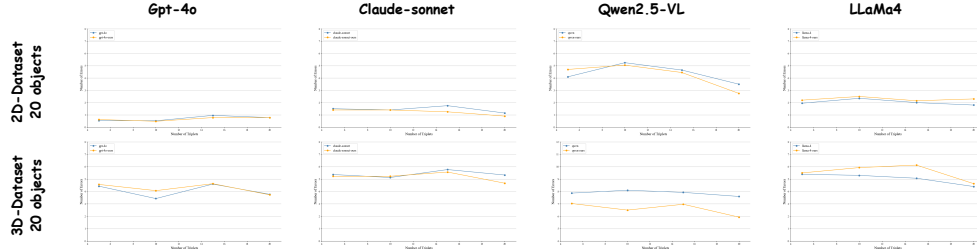


Figure 7: Results of the 10 objects Scene Description task across varying numbers of triplets for 2D and 3D scenes, using different VLM models (GPT-4o, Claude-Sonnet, Qwen2.5-VL, and LLaMa4).

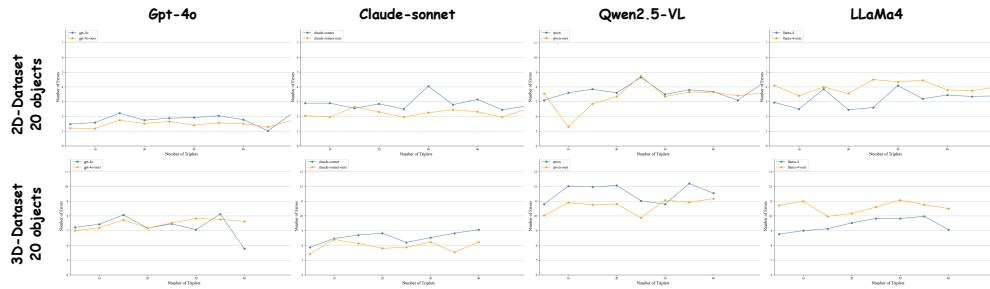


Figure 8: Results of the 15 objects Scene Description task across varying numbers of triplets for 2D and 3D scenes, using different VLM models (GPT-4o, Claude-Sonnet, Qwen2.5-VL, and LLaMa4).

2D Scenes: We generated 200 synthetic 2D scenes with controlled object configurations. For each scene, we created multiple-choice questions testing spatial relationships (top-left, top-right, bottom-left, bottom-right).

3D Scenes: Similarly, we produced 200 synthetic 3D scenes with three-dimensional arrangements, following the same question generation protocol as the 2D scenes.

For real-world evaluation, we used 200 natural images from the benchmark [38], which provides diverse object arrangements in unconstrained environments.

This approach enables systematic assessment of spatial reasoning across: (1) fundamental 2D relationships, (2) complex 3D configurations, and (3) real-world scenarios.

C.2 Score Metrics

To evaluate the performance of different models across visual reasoning tasks, we employ five metrics: Edit Distance, Accuracy, F1 score, Jaccard Similarity, and Mean Squared Error (MSE). Each metric is applied according to the nature of the task, and formal definitions are provided below.

1. Edit Distance (Scene Description)

For the scene description task (both 2D and 3D), we define a custom edit distance that penalizes discrepancies between the predicted and ground truth object lists. The metric is computed in the following steps:

1. **Exact Matches:** All objects with matching *shape* and *color* are removed from both sets.
2. **Partial Matches:**
 - Objects with the same shape but different colors incur a penalty of 1.
 - Objects with the same color but different shapes incur a penalty of 1.
3. **Missed Ground Truth Objects:** Any remaining unmatched ground truth objects are penalized with 2 points.

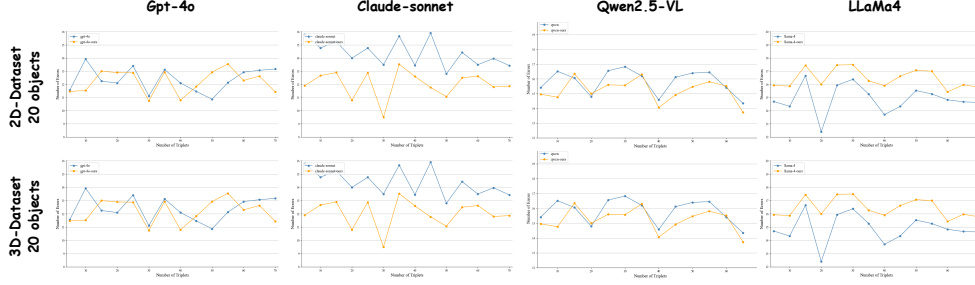


Figure 9: Results of the 20 objects Scene Description task across varying numbers of triplets for 2D and 3D scenes, using different VLM models (GPT-4o, Claude-Sonnet, Qwen2.5-VL, and LLaMa4).

The total edit distance is calculated as:

$$\text{EditDistance} = 1 \times N_{\text{partial}} + 2 \times N_{\text{missed}} \quad (2)$$

where N_{partial} is the number of shape-only or color-only matches, and N_{missed} is the count of completely missed objects. This asymmetric formulation reflects the observation that models more often miss objects than hallucinate them.

2. Accuracy (Visual Search, Counting, Spatial Relationship)

Accuracy is used for classification-based tasks and is defined as the ratio of correct predictions to total predictions:

$$\text{Accuracy} = \frac{N_{\text{correct}}}{N_{\text{total}}} \quad (3)$$

This metric is used in visual search, counting and spatial relationship evaluations.

3. F1 Score (Reasoning Trace Evaluation)

F1 score measures the harmonic mean between precision and recall and is particularly useful for object-level evaluation:

$$\text{F1} = 2 \cdot \frac{\text{Precision} \cdot \text{Recall}}{\text{Precision} + \text{Recall}} \quad (4)$$

with:

$$\text{Precision} = \frac{TP}{TP + FP}, \quad \text{Recall} = \frac{TP}{TP + FN} \quad (5)$$

where TP (true positives) are objects correctly predicted with matching shape and color, FP (false positives) are incorrect predictions, and FN (false negatives) are missed objects.

4. Jaccard Similarity (Reasoning Trace Evaluation)

Jaccard similarity measures the set-level overlap between prediction and ground truth:

$$\text{Jaccard} = \frac{|P \cap G|}{|P \cup G|} \quad (6)$$

where P and G are the sets of predicted and ground truth objects respectively, and equality requires both shape and color to match.

5. Mean Squared Error (Counting)

For the counting task, we compute the mean squared error (MSE) between the predicted and true object counts:

$$\text{MSE} = \frac{1}{N} \sum_{i=1}^N (\hat{y}_i - y_i)^2 \quad (7)$$

Table 6: Mean squared error (MSE) of counting task across GPT-4o, Claude3.5-sonnet, LLaMa4, and Qwen2.5-VL on 2D, 3D and natural image datasets using base models and our method.

	GPT-4o		Claude-sonnet		LLaMa4		Qwen2.5-VL	
	Simple	Ours	Simple	Ours	Simple	Ours	Simple	Ours
2D	7.50	1.33	5.32	5.25	5.515	5.575	15.03	3.89
3D	6.13	2.44	2.28	3.01	2.74	1.53	22.04	6.21
Natural	37.33	6.33	1048.63	42.20	6.30	5.89	35.10	24.32

where \hat{y}_i is the predicted count and y_i is the ground truth count for scene i , and N is the total number of scenes. MSE penalizes large deviations in count predictions more heavily.

MSE Results: Table 6 presents the Mean Squared Error (MSE) for object counting across the evaluated models. While our primary analysis focused on accuracy metrics, the MSE results provide complementary insights, particularly regarding the magnitude of counting errors.

Our method demonstrates consistent error reduction compared to baseline performance. The most notable improvements occur in natural image scenarios, where exact count prediction remains challenging but our approach achieves substantial MSE reduction (Claude3.5-sonnet: 42.20 versus 1048.63). Similar improvements are evident in synthetic environments, with GPT-4o (1.33 versus 7.50 in 2D) and Qwen2.5-VL (3.89 versus 15.03 in 2D; 6.21 versus 22.04 in 3D) showing significant decreases in squared error.

These MSE results complement our accuracy findings by demonstrating that our method not only increases correct predictions but also reduces the severity of counting errors when they occur. The notable MSE improvement on natural images, despite the inherent difficulty of exact counting in real-world scenes, highlights our method’s ability to prevent large counting deviations.

D Implementation Details

In this section, we describe the prompts used across our four evaluation tasks. While we maintain a consistent prompt template for all models, each task requires a tailored instantiation to address its specific objectives. In Figures 10, 11, 12, and 13, we detail the exact prompt formulations employed for each task, which produce the results reported in the Experiments section. Additionally, to assess the model’s Chain-of-Thought (CoT) reasoning ability, we prepend “Let’s think step by step . . .” to each prompt, encouraging the model to articulate intermediate reasoning before arriving at its final prediction.

E Input and Output examples

In this section, we provide a series of examples to demonstrate the outputs of our row-wise structure across different tasks, including visual search, counting, scene description, and spatial relationship analysis. Each task is illustrated with both synthetic (2D and 3D) and, where applicable, real-world scenes. For each task, we compare the outputs of applying our method with those of a baseline model, highlighting the impact of our approach on a VLM.

E.1 Visual Search

For the visual search task, we present input and output examples from both 2D and 3D datasets (shown in Figures 14 and 15, respectively). In the first example (Figure 14), the objective was to locate the green ‘L’ among a set of ‘L’ and ‘T’ letters within the scene. The baseline model failed to detect the target, returning a [False] output. In contrast, applying row-wise structure successfully identified the green ‘L’ and returned a [True] output, demonstrating its effectiveness. This pattern was similarly observed in the 3D scene, where the baseline model again failed to locate the target object, while applying our method accurately detected the presence of the described object within the scene.

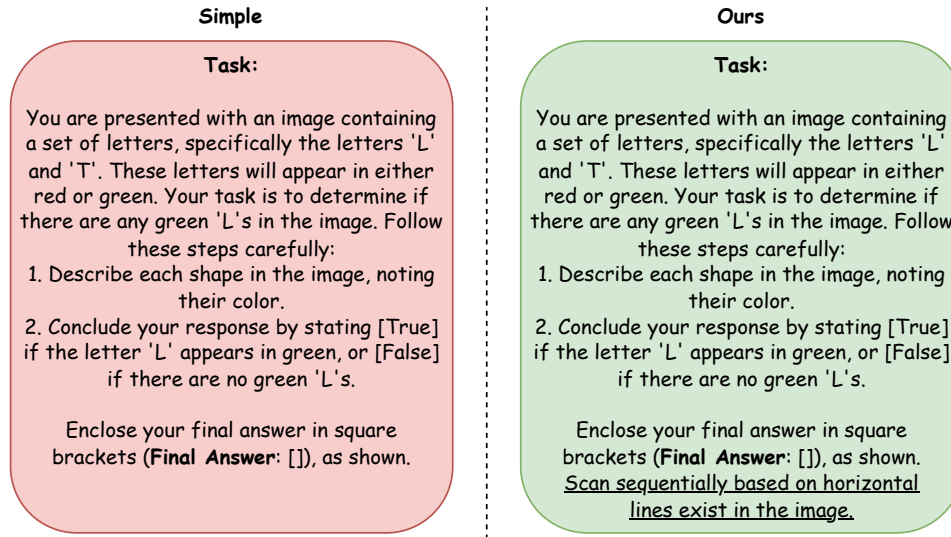


Figure 10: Displaying the prompt used for the 2D scenes in the visual search task. The only difference between the two prompts is the additional instruction: “Scan sequentially based on horizontal lines exist in the image.”

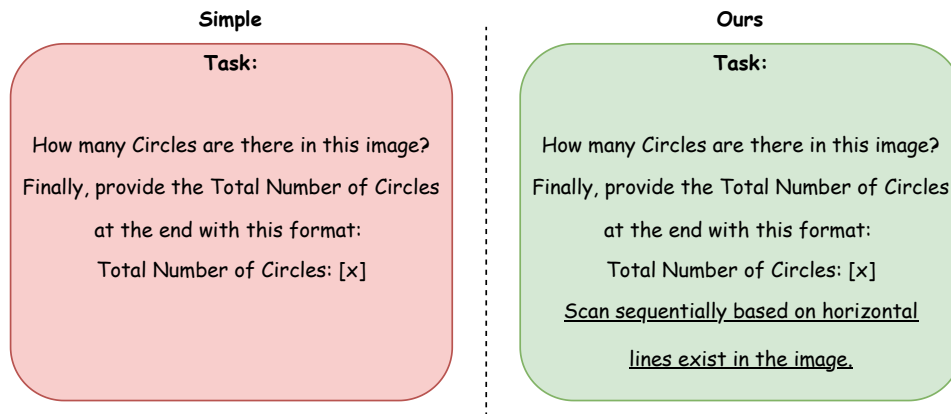


Figure 11: Displaying the prompt used for the 2D scenes in the counting task. The phrase “Scan sequentially based on horizontal lines exist in the image” is added to our prompts, in contrast to the simple input.

E.2 Counting

For the counting task, in addition to the 2D and 3D scene examples, we incorporate a sample from the natural-image dataset utilized in the evaluation of “Learning to Count Everything” [32]. The corresponding examples are presented in Figures 16, 17, and 18, respectively. In all three cases, the VLM model misses some objects or hallucinates extra objects and inaccurately counts the number of objects. In contrast, when our proposed method is applied, the VLM model provides the correct object count.

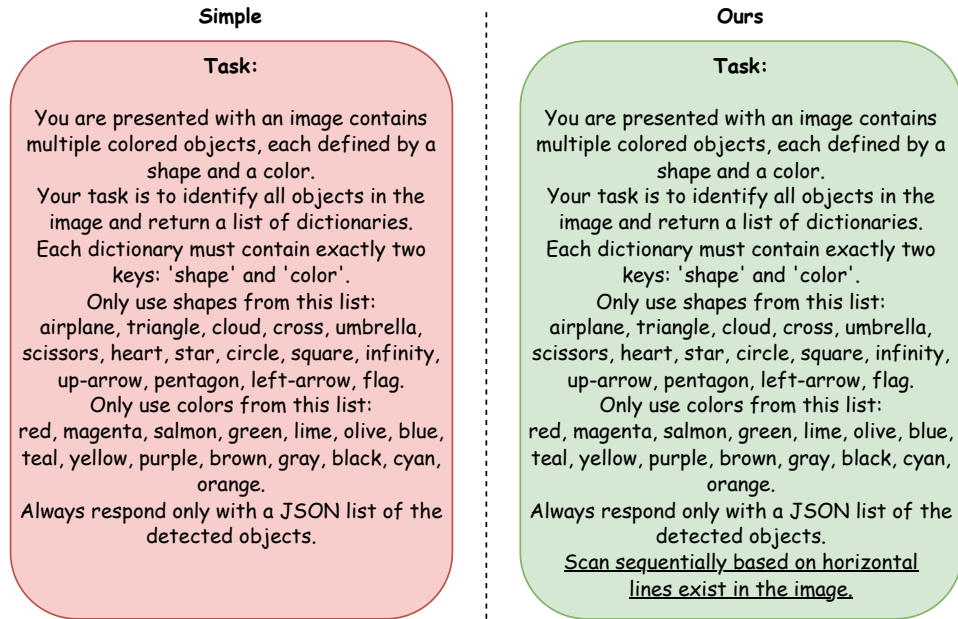


Figure 12: Showing the prompt used in our 2D scene description task. The phrase “Scan sequentially based on horizontal lines exist in the image” is the only addition to our prompt.

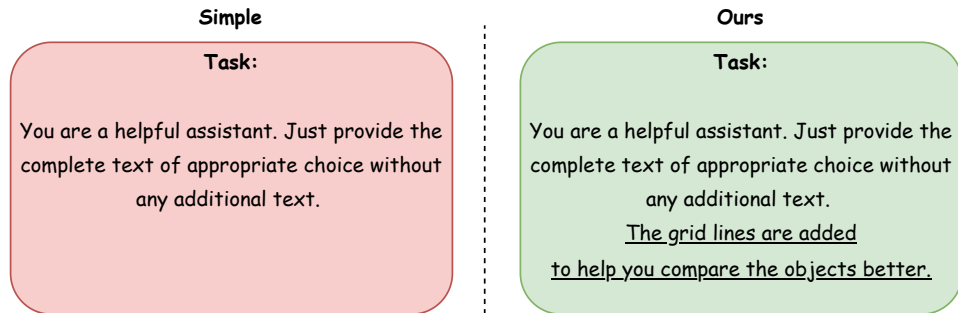


Figure 13: Showing the prompt that we use in the 2D scenes for the spatial relationship task. The only difference from the baseline is the added instruction: “The grid lines are added to help you compare the objects better.”

E.3 Scene Description

In Figures 19 and 20, we present two synthetic examples (one from a 2D scene and the other from a 3D scene) both relevant to the scene description task. The VLM initially fails to accurately identify all objects and their respective attributes within the scenes. However, by applying our proposed method, we improve the model’s performance, enabling it to more accurately and precisely describe the objects in the scenes.

E.4 Spatial Relationship

For the spatial relationship task, we present three examples: one from a 2D synthetic scene (Figure 21), one from a 3D synthetic scene (Figure 22), and one from the natural Spatial Reasoning dataset [38] (Figure 23). In all of these examples, the VLM initially selects the wrong choice. However, adding

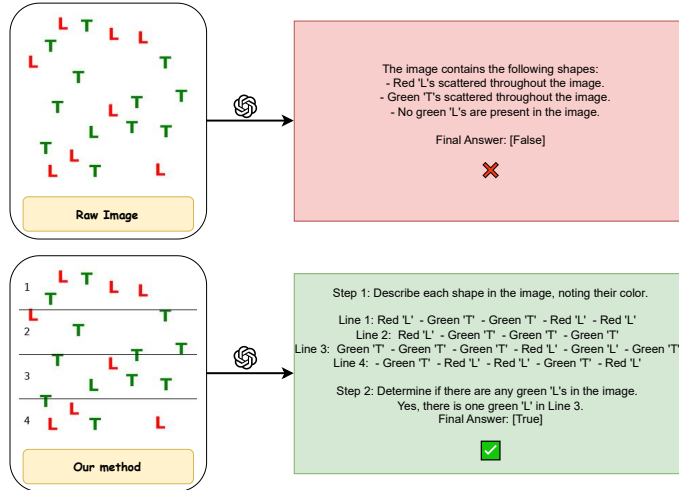


Figure 14: An example of a 2D visual search task illustrating the impact of our proposed method on the output of the VLM model. The baseline fails to detect the green 'L', returning [False], while our row-wise structure successfully identifies it.

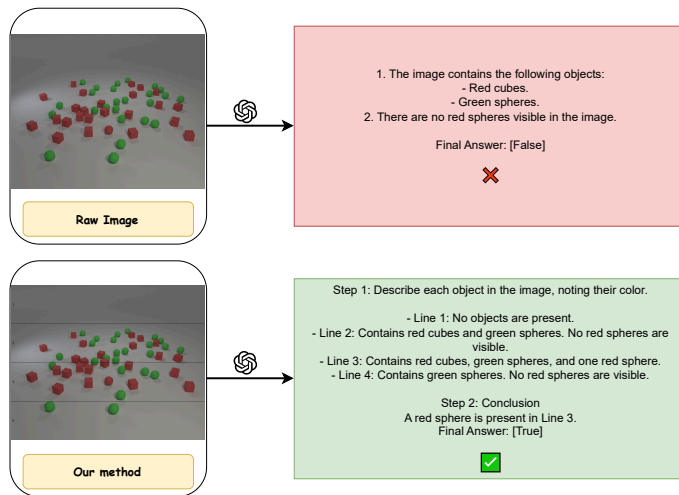


Figure 15: An example of a 3D visual search task illustrating the impact of our row-wise structure on the VLM model's output. The baseline fails to detect the red sphere, returning [False], while applying our method successfully detects it and returns [True].

grid lines helps the model better compare the spatial relationships between the objects, leading to more accurate answers.

F Attention visualization

In this section, we analyze and visualize the attention maps corresponding to the generated outputs from both the baseline and our proposed method using the Qwen2.5-VL-7B-Instruct [41] model.

Figure 24 shows the results of our method, where we instruct the model to "Scan sequentially based on horizontal lines exist in the image," encouraging it to analyze each row independently. The extracted attention maps for each predicted numerical value confirm this approach, demonstrating that the model attends more strongly to the corresponding spatial regions. For comparison, Figure 25 presents the results from the baseline model, which was given the same instruction. In this case, the attention is less focused, and the predicted numbers do not align clearly with their respective regions.

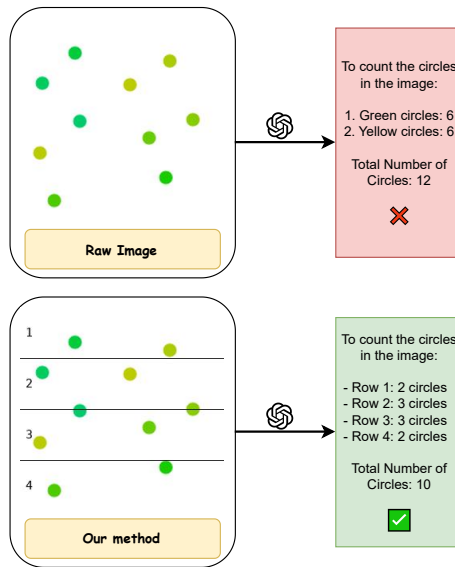


Figure 16: An example of a 2D counting task and the impact of our proposed method on the output of the VLM model. The baseline approach incorrectly counts the number of circles in the 2D scene, whereas our row-wise structure method enables the VLM to accurately count the number of circles.

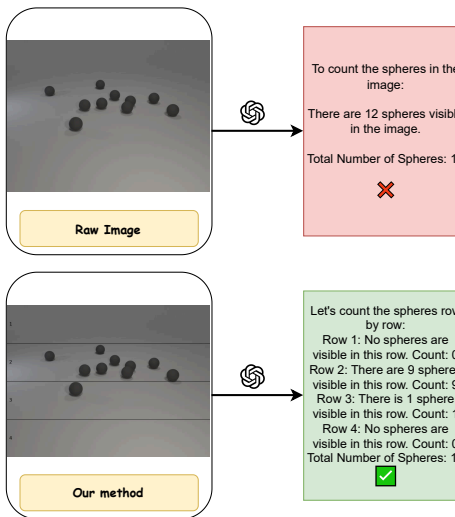


Figure 17: An example of a 3D counting task and the impact of our proposed method on the VLM model's output. The baseline method inaccurately counts the number of spheres in the 3D scene, whereas applying our method enables the VLM to accurately count the number of spheres.

This shows that adding the horizontal line guidance enhanced the model's ability to focus on each region independently, resulting in improved performance and greater precision.

By applying our method, the model is guided to focus sequentially on smaller, more localized regions within the image. This enables it to more accurately identify and attend to objects in specific areas. The localized approach allows for a more detailed and focused analysis, leading to better alignment between the predicted numerical values and the corresponding spatial regions. In contrast, the baseline method attempts to attend to the entire image in a single step, without such localized guidance. This

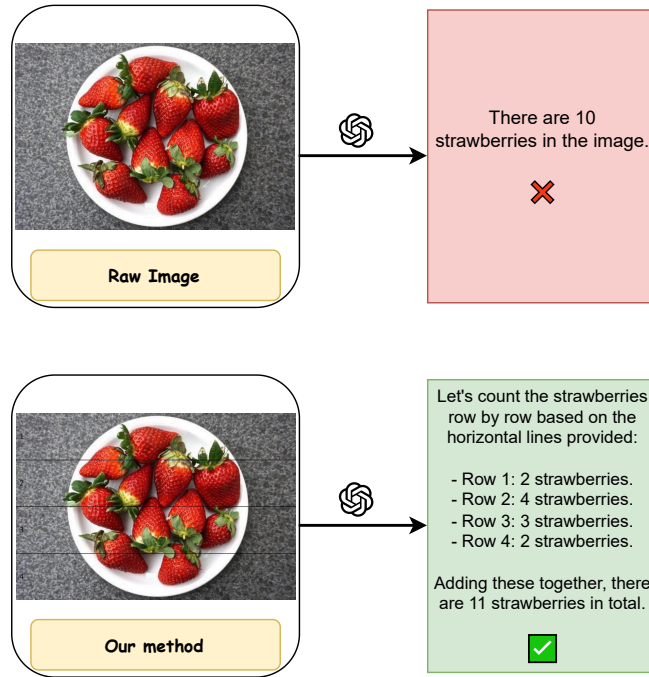


Figure 18: An example of a natural dataset for the counting task and the impact of our proposed method on the output of the VLM model. The baseline method fails to accurately count the number of strawberries in the dataset, whereas row-wise structure enhances the VLM’s ability to determine the strawberry count correctly.

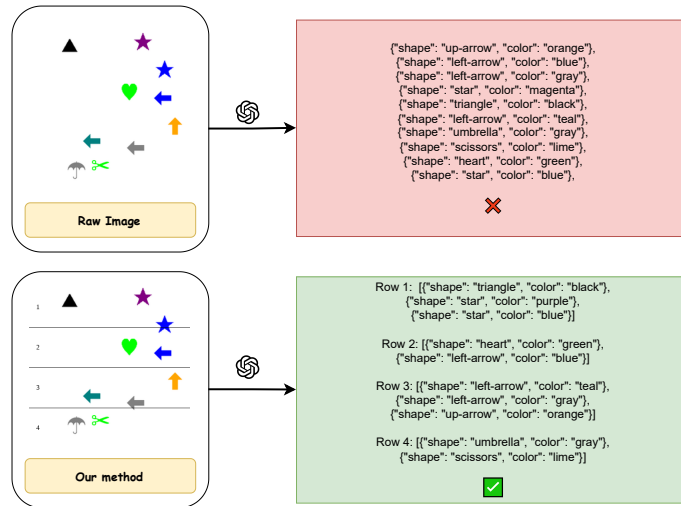


Figure 19: An example of a 2D scene description task and the impact of our method on the VLM’s output. The VLM fails to describe the purple star shape in the scene, whereas our method correctly describes all the objects.

broader attention scope reduces the model’s ability to focus on specific regions, causing difficulty with precise object identification and reducing accuracy. The model fails to effectively resolve finer details and spatial relationships within the image. To further illustrate this, Figure 26 shows the baseline’s

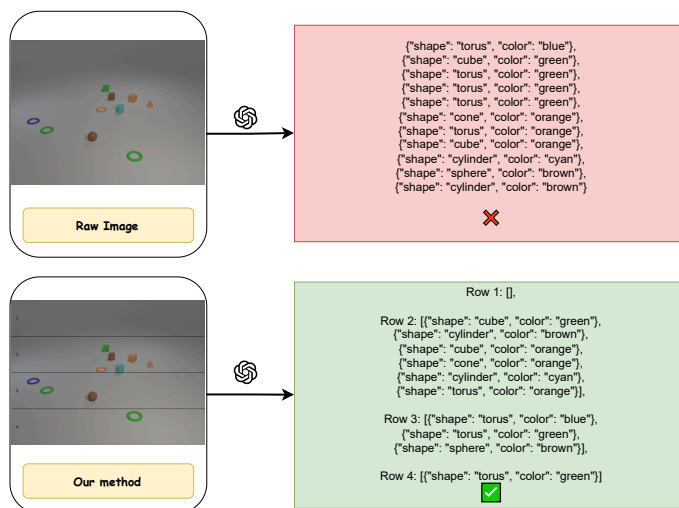


Figure 20: An example of a 3D scene description task and the improvement gained by applying our method. The VLM incorrectly adds an extra object, counting three green toruses instead of two, which aren't part of the scene. In contrast, our proposed method accurately describes only the objects present.

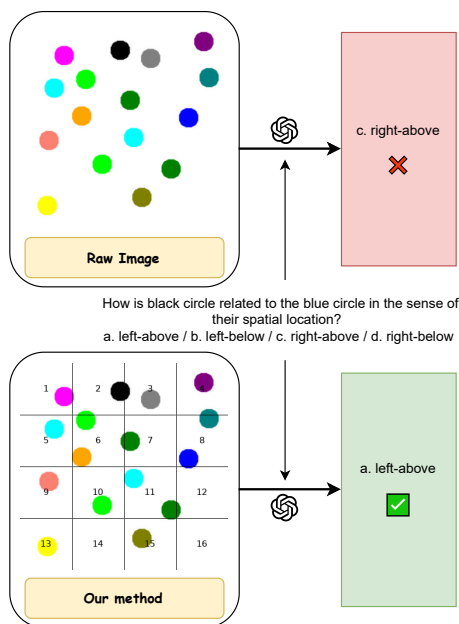


Figure 21: An example of a 2D spatial relationship task and the effect of applying our proposed method on the VLM's output. As shown in the figure, adding grid lines assists the VLM in selecting the correct choice.

predicted numbers, which attempt to attend to all circles simultaneously. Due to the high number of circles, the model fails to answer the question correctly. Conversely, Figure 24 demonstrates that by incorporating explicit sequential reasoning, our method allows the model to count objects in each region more accurately and aggregate the results more effectively.

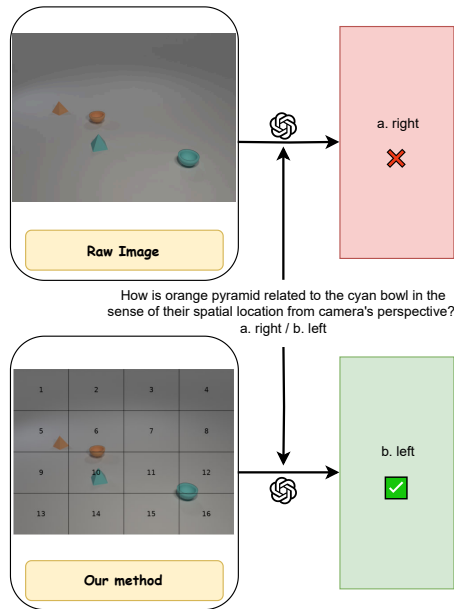


Figure 22: An example of a 3D spatial relationship task and the impact of applying our method on the VLM's output. As shown in the figure, adding grid lines improves the VLM's ability to select the correct choice.

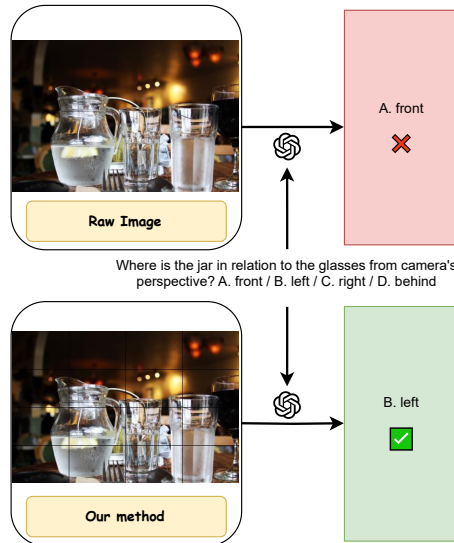


Figure 23: An example from a natural dataset for the spatial relationship task and the impact of applying our method on the VLM's output. The question asks about the spatial relationship between the jar and glasses from the camera's perspective. As shown in the figure, applying our method helps the VLM answer the question correctly.

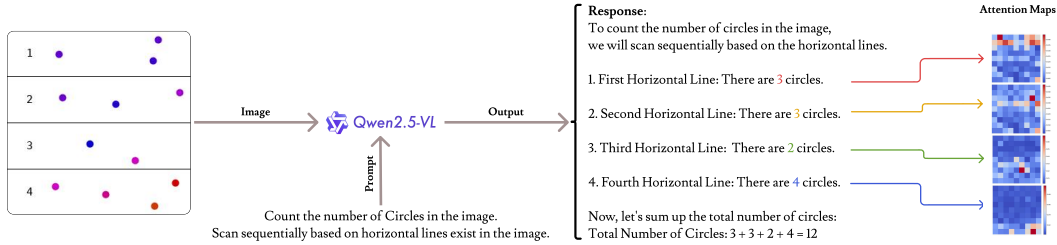


Figure 24: Visualization of 2D attention maps generated by our proposed method using the Qwen2.5-VL-7B-Instruct model on a counting task. The attention patterns demonstrate that the predicted numerical values for each row attend more strongly to their corresponding spatial regions, indicating improved alignment between predictions and visual content.

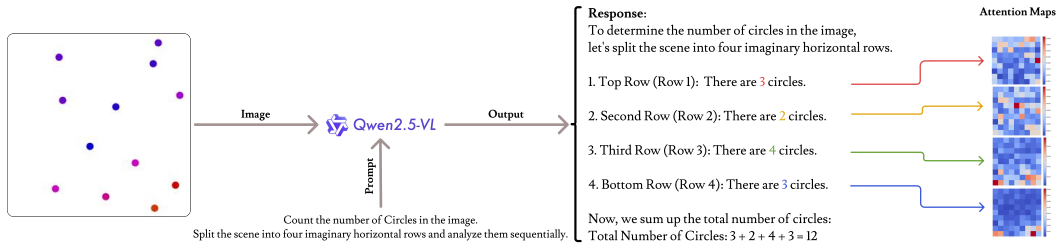


Figure 25: Visualization of 2D attention maps generated by the baseline method using the Qwen2.5-VL-7B-Instruct model on the same counting task. Although provided with the same instruction to scan the image row by row, the attention maps exhibit less focus, and the predicted numerical values show weaker alignment with their corresponding spatial regions. Additionally, the numerical predictions lack proper row-region binding, and the predictions for the third and fourth rows are incorrect.

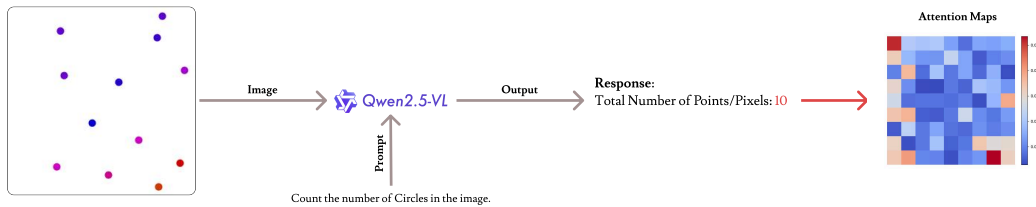


Figure 26: Visualization of the 2D attention maps generated by the baseline method using the Qwen2.5-VL-7B-Instruct model on a counting task. The attention maps reveal a broader, less focused attention pattern, with the model attempting to attend to all regions simultaneously. This lack of localized attention results in incorrect predictions, as evidenced by the model's failure to properly align with the specific spatial regions in the image, leading to errors in counting.

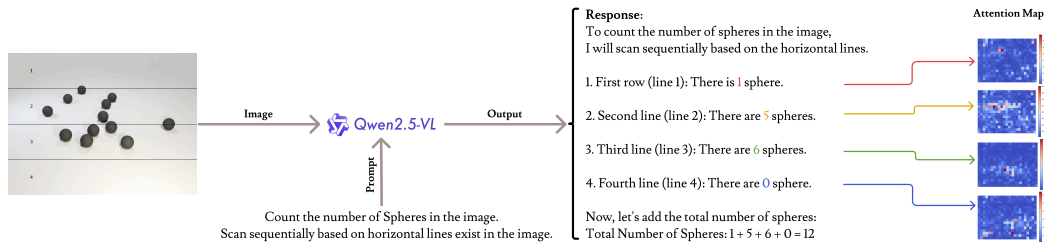


Figure 27: Visualization of 3D attention maps generated by our proposed method using the Qwen2.5-VL-7B-Instruct model on a counting task. The attention patterns demonstrate that the predicted numerical values for each row attend more strongly to their corresponding spatial regions, indicating improved alignment between predictions and visual content.